

Revised onset age of magnetochron M0r: Chronostratigraphic and geologic implications

Youjuan Li¹, Huafeng Qin², Brian R. Jicha¹, Magdalena H. Huyskens³, Corey J. Wall⁴, Robin B. Traylor^{4,5}, Qing-Zhu Yin³, Mark Schmitz⁴, Yongxin Pan⁶, Chenglong Deng², Brad S. Singer¹, Huaiyu He^{2,*}, and Rixiang Zhu²

¹Department of Geoscience, University of Wisconsin–Madison, Madison, Wisconsin 53706, USA

²State Key Laboratory of Lithospheric Evolution, Institute of Geology and Geophysics, Chinese Academy of Sciences, Beijing 100029, China

³Department of Earth and Planetary Sciences, University of California, Davis, California 95616, USA

⁴Department of Geosciences, Boise State University, Boise, Idaho 83725, USA

⁵Department of Life and Environmental Sciences, University of California, Merced, California 95343, USA

⁶Key Laboratory of Earth and Planetary Physics, Institute of Geology and Geophysics, Chinese Academy of Sciences, Beijing 100029, China

ABSTRACT

The timing of the onset of magnetochron M0r and its duration are disputed, reflecting both a limited set of radioisotopic dates and uncertain magnetostratigraphic correlations. We present a chronostratigraphic framework for a reversed polarity interval based on two chronometers (⁴⁰Ar/³⁹Ar, U-Pb) and newly published paleomagnetic data from the Qingshan Group, Jiaolai Basin, China. Bayesian modeling of U-Pb zircon and ⁴⁰Ar/³⁹Ar sanidine dates suggests a minimum duration of 540 ± 37 k.y. (95% credible interval) for the reversed polarity interval. These findings are compatible with an astrochronologic age model for M-sequence seafloor magnetic anomalies, indicating that the reversely magnetized sediments correspond to magnetochron M0r rather than the shorter chron “M-1r.” Integration of U-Pb and ⁴⁰Ar/³⁹Ar ages constrains the onset of M0r to 120.29 ± 0.09 Ma, which is ~1 m.y. younger than that inferred in the current geologic time scale (GTS 2020). This finding also implies that the Cretaceous normal superchron (CNS) began at 119.70 ± 0.12 Ma and that the average seafloor spreading rate during the CNS was ~3.5% higher than that inferred from GTS 2020. It also suggests that oceanic anoxic event 1a began at 119.40 ± 0.12 Ma, thereby providing an updated chronologic basis for exploring the primary trigger of this carbon cycle perturbation.

INTRODUCTION

The base of magnetic polarity chron M0r is a proposed marker for the Barremian-Aptian boundary, and its top marks the onset of the “quiet” Cretaceous normal superchron (CNS; e.g., Helsley and Steiner, 1968; Gale et al., 2020; Zhang et al., 2021). The precise onset of chron M0r and its duration are thus crucial factors for constraining past oceanic, tectonic, and geodynamic behavior. Oceanic anoxic event 1a (OAE 1a), a major paleoceanographic and paleoclimatic event, began ~780 k.y. after the onset of chron M0r (Malinverno et al., 2010), and it is inferred to have been associated with volcanism

that built the Ontong Java Nui Plateau (Tejada et al., 2009; Erba et al., 2015). Magnetochron M0r is the youngest end of the M-sequence magnetic anomalies, and its onset is a key tie point to reconstruct global spreading rates and correlative major plate-tectonic events (Malinverno et al., 2012). Moreover, the Early Cretaceous was a period of amplified igneous activity, so precise dating of M0r is necessary for understanding the relationship between plume-plate and magmatic-biotic processes (Santosh, 2010).


Despite numerous efforts to determine the timing of chron M0r in submarine and terrestrial archives (e.g., Pringle and Duncan, 1995; Chambers et al., 2004; He et al., 2008; Malinverno et al., 2012; Olierook et al., 2019; Zhang et al., 2021; Leandro et al., 2022), its precise onset age and duration remain uncertain. Qin et al. (2022)

reported a paleomagnetic reversal within the Qingshan Group in Jiaodong Peninsula, eastern China, and provided a laser ablation–inductively coupled plasma–mass spectrometry (LA-ICP-MS) U-Pb age of 121.3 ± 2.8 Ma. The U-Pb age from Qin et al. (2022) is nearly identical to the chron M0r onset age of 121.4 Ma in the current geologic time scale (GTS 2020; Gale et al., 2020), but it is imprecise and not anchored in a high-resolution chronostratigraphic framework.

We present U-Pb zircon dates using both chemical abrasion–isotope dilution–thermal ionization mass spectrometry (CA-ID-TIMS) and chemical abrasion–isotope dilution–isotope ratio mass spectrometry (CA-ID-IRMS), plus ⁴⁰Ar/³⁹Ar single sanidine fusion dates, from four tuffs in the Qingshan Group. Pairs of tuffs are located at the base and near the uppermost exposure of the reversed polarity interval, respectively, allowing for the onset and minimum duration of chron M0r to be constrained. Moreover, our revised onset age of chron M0r has implications for the timing of the CNS, OAE 1a, and the potential driver for the latter.

GEOLOGIC BACKGROUND AND SAMPLING

The 12,000 km² late Mesozoic Jiaolai Basin in Shandong Province, eastern China, is a fault-controlled feature composed of Cretaceous–Cenozoic volcanic rocks and fluvial-lacustrine deposits (Fig. 1A; Zhang et al., 2003). From bottom to top, the Cretaceous–Cenozoic strata are divided into the Laiyang, Qingshan, and Wangshi Groups (Fig. 1B). The Laiyang and Wangshi groups are dominated by clastic deposits,

Youjuan Li  <https://orcid.org/0000-0002-1126-3258>
*huaiyuhe@mail.iggcas.ac.cn

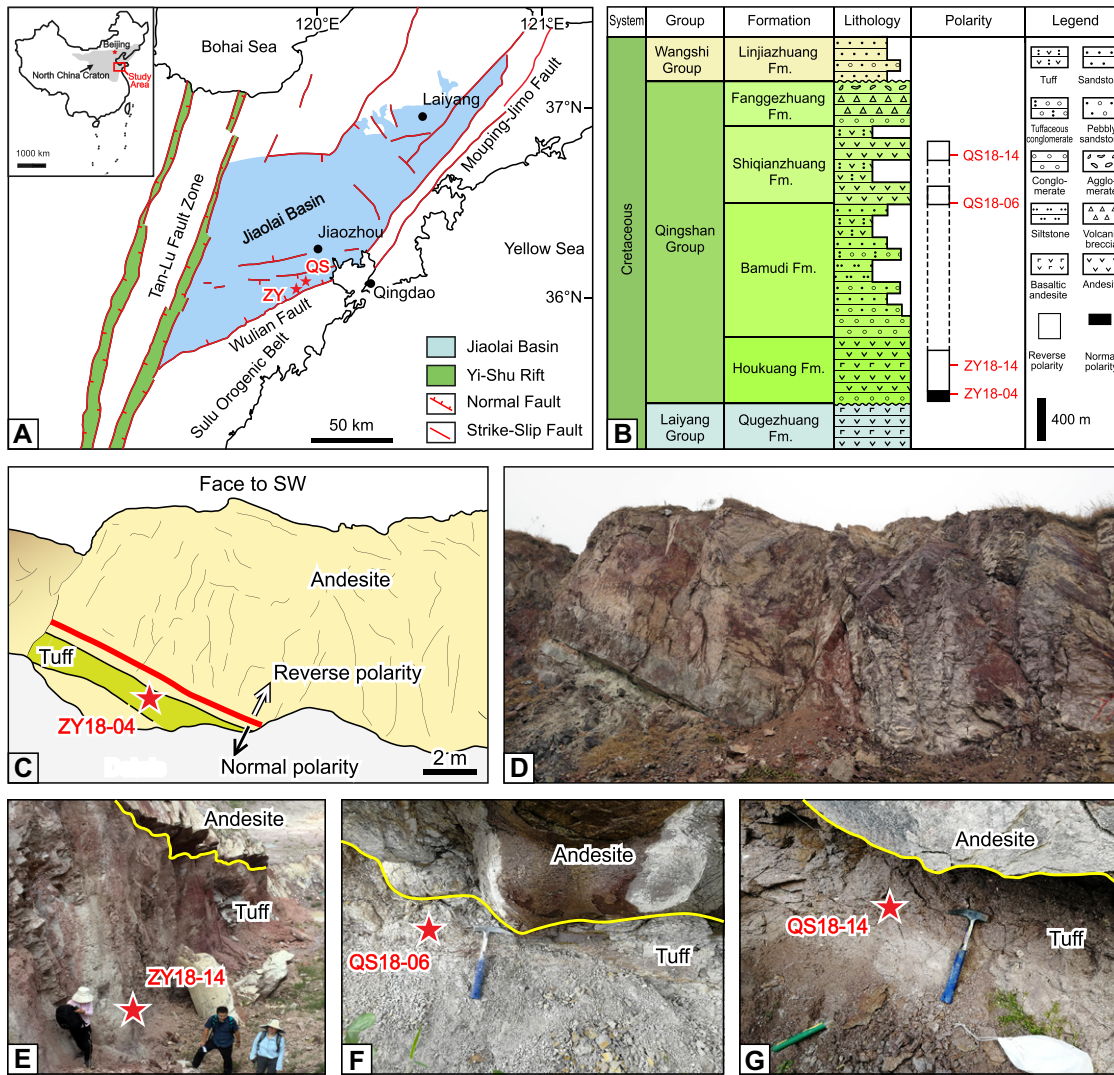


Figure 1. (A) Setting of Jiaolai Basin. (B) Stratigraphic and paleomagnetic sections in Qingshan Group. Fm—Formation. (C) Sketch of part D. (D–G) Field photos. Parts A and B are modified after Qin et al. (2022). ZY—Zhangying; QS—Qingshan.

whereas the Qingshan Group is characterized by silicic lava and pyroclastic rocks interbedded with sedimentary rocks. The Qingshan Group is composed of the Houkuang, Bamudi, Shiqianzhuang, and Fanggezhuang Formations (Fig. 1B). The Bamudi Formation mainly consists of conglomerate and sandstone intercalated with trachyandesite, and the Houkuang, Shiqianzhuang, and Fanggezhuang Formations are dominated by andesite and rhyolitic tuffs (Qin et al., 2022). A magnetic reversal occurs within the lower part of the Houkuang Formation (Fig. 1B), and tuff ZY18-04 previously yielded an LA-ICP-MS U-Pb age of 121.3 ± 2.8 Ma for the normal-to-reverse polarity change (Qin et al., 2022).

We undertook $^{40}\text{Ar}/^{39}\text{Ar}$ sanidine and U-Pb zircon dating of four tuffs: (1) ZY18-04 is ~90 cm thick and ~15 cm below the magnetic polarity boundary (Figs. 1C–1D; Qin et al., 2022), (2) ZY18-14 is an ~4-m-thick reddish white tuff (Fig. 1E), (3) QS18-06 is an ~2.5-cm-thick beige tuff, and (4) QS18-14 is an ~30-cm-thick reddish brown tuff (Figs. 1F and 1G).

RESULTS AND DISCUSSION

Uncertainties for calculated weighted mean ages are reported at the 95% confidence level in the $\pm X(Y)[Z]$ format, where X is the analytical uncertainty, Y is the combined analytical and tracer (U-Pb) or J uncertainty ($^{40}\text{Ar}/^{39}\text{Ar}$), and Z is analytical and tracer (or J value) and ^{238}U (U-Pb) or ^{40}K ($^{40}\text{Ar}/^{39}\text{Ar}$) decay constant uncertainties (Fig. 2). Complete U-Pb and $^{40}\text{Ar}/^{39}\text{Ar}$ isotopic data supporting the ages in Figures 2A and 2B are provided in Supplemental Tables S1, S3, S4, and S5.¹

¹Supplemental Material. Text S1: U-Pb, $^{40}\text{Ar}/^{39}\text{Ar}$, and Bayesian modeling analytical methods. Table S1: Summary of radioisotopic ages from Qingshan Group, Jiaolai Basin, China. Table S2: Summary of ages determined for Barremian-Aptian boundary and chron M0r. Tables S3, S4, and S5: Complete U-Pb CA-ID-IRMS, CA-ID-TIMS, and $^{40}\text{Ar}/^{39}\text{Ar}$ data from three different laboratories. Please visit <https://doi.org/10.1130/GEOL.S.22310293> to access the supplemental material, and contact editing@geosociety.org with any questions.

Eight of 13 zircon crystals from sample ZY18-04 analyzed by CA-ID-IRMS at the University of California, Davis (UCD), California, yielded a weighted mean $^{206}\text{Pb}/^{238}\text{U}$ date of $120.276 \pm 0.024(0.044)[0.136]$ Ma (mean square of weighted deviates [MSWD] = 1.21). At Boise State University (BSU), Boise, Idaho, the youngest five of 13 crystals analyzed by CA-ID-TIMS were concordant and yielded a weighted mean $^{206}\text{Pb}/^{238}\text{U}$ age of $120.296 \pm 0.026(0.045)[0.137]$ Ma (MSWD = 1.97). At the University of Wisconsin, Madison, Wisconsin, WiscAr laboratory (WiscAr), the youngest 40 of 58 single-crystal sanidine fusion dates from ZY18-04 yielded >98% radiogenic $^{40}\text{Ar}^*$ and gave a weighted mean age of $120.292 \pm 0.040(0.078)[0.222]$ Ma (MSWD = 1.02).

The youngest six of nine $^{206}\text{Pb}/^{238}\text{U}$ CA-ID-IRMS dates from ZY18-14 were concordant and yielded a weighted mean age of $120.034 \pm 0.070(0.079)[0.151]$ Ma (MSWD = 0.34), which we interpret as the eruption age. The youngest 21 of 34 single-crystal total fusion sanidine analyses from QS18-06 yielded

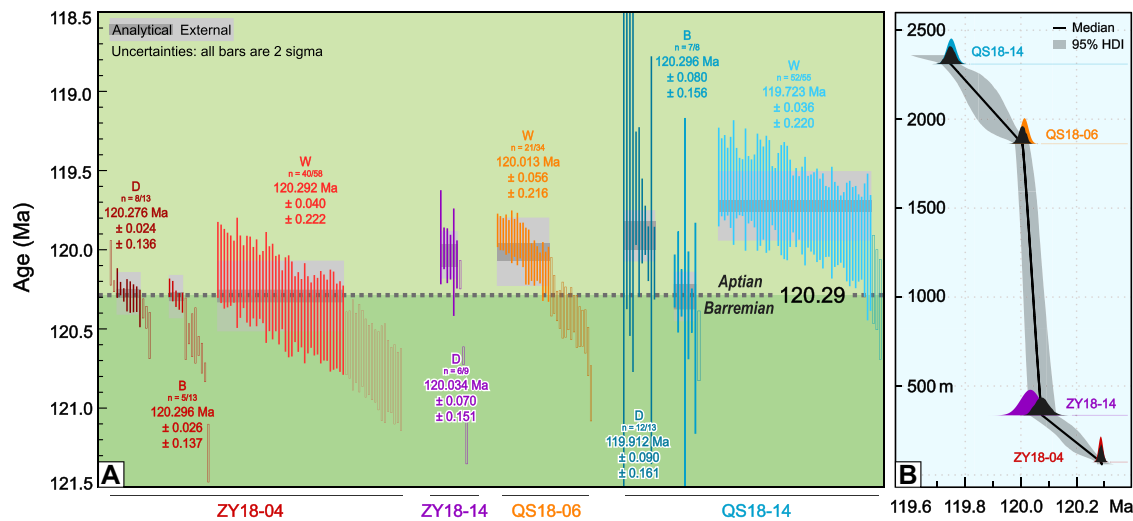


Figure 2. (A) Rank-order plot of U-Pb and $^{40}\text{Ar}/^{39}\text{Ar}$ dates from Qingshan Group. Open bars denote analyses excluded from weighted mean age calculations. (B) Age-depth model: $^{40}\text{Ar}/^{39}\text{Ar}$ and U-Pb dates were integrated into four tuff age likelihood inputs into Bayesian modeling. Posterior distributions are superimposed in black on original likelihoods in color. D—University of California–Davis U-Pb dates; B—Boise State University U-Pb dates; W—University of Wisconsin–Madison (WiscAr) $^{40}\text{Ar}/^{39}\text{Ar}$ dates.

a weighted mean age of $120.013 \pm 0.056(0.058)$ [0.216] Ma (MSWD = 0.89). For QS18-14, 12 of 13 zircons measured at UCD were concordant and yielded a weighted mean $^{206}\text{Pb}/^{238}\text{U}$ age of $119.912 \pm 0.090(0.097)$ [0.161] Ma (MSWD = 1.16). At BSU, the youngest seven of eight zircons in QS18-14 yielded a weighted mean age of $120.296 \pm 0.080(0.088)$ [0.156] Ma (MSWD = 0.65). The youngest 52 of 55 sanidine dates from QS18-14 yielded a weighted mean age of $119.723 \pm 0.036(0.076)$ [0.220] Ma (MSWD = 0.84).

For sample ZY18-04, the U-Pb and $^{40}\text{Ar}/^{39}\text{Ar}$ dates from the three laboratories are indistinguishable within uncertainties (Figs. 2A and 2B), so a weighted mean age of $120.287 \pm 0.016(0.030)$ [0.088] Ma represents the time since deposition. As ZY18-04 is located ~ 15 cm below the magnetic polarity boundary, its age tightly constrains the base of the reversed polarity interval.

Sample QS18-14 yielded two age populations (Fig. 2A); we interpret the older dates from BSU and the three oldest $^{40}\text{Ar}/^{39}\text{Ar}$ dates to reflect reworking or xenocrystic contamination. The U-Pb age from UCD and $^{40}\text{Ar}/^{39}\text{Ar}$ age from the younger population are consistent and thus are interpreted to reflect the time since deposition. The first reversed polarity interval recognized within the CNS, the ISEA (also called “M-1r”; VandenBerg et al., 1978), occurs near the base of the *Globigerinelloides algerianus* zone (Keating and Helsley, 1978; Cronin et al., 2001) with an inferred duration of < 100 k.y. (Tarduno, 1990). In contrast, astronomical calibration of Italian reference sections suggests that chron M0r lasted ~ 500 k.y. (Huang et al., 2010). Spreading rate constraints on the geomagnetic polarity time scale suggest a duration of 370 k.y. (Ogg, 2012). Malinverno et al. (2010) estimated the duration of chron M0r at 490 ± 100 k.y. (2σ) from cyclostratigraphy of the Cismon section, Italy. By integrating magnetostratigraphic

from cyclostratigraphy with the marine magnetic anomaly record, Malinverno et al. (2012) suggested a duration of 590 ± 82 k.y. (2σ) for M0r. Leandro et al. (2022) proposed a 420 k.y. duration for M0r using astronomical tuning of the Poggio le Guaine core, Italy; however, the uncertainty of this estimate has not been quantified. Bayesian age models (Trayler et al., 2020) using our Qingshan Group results established an internally consistent chronostratigraphic framework that tightly constrains the age of reversely magnetized strata (Fig. 2B). Our U-Pb findings suggest that the reversed polarity interval in the Qingshan Group records a duration of 412 ± 83 k.y. between an onset at 120.286 ± 0.018 Ma and termination at 119.912 ± 0.090 Ma. The $^{40}\text{Ar}/^{39}\text{Ar}$ dates from the same tuffs span from

120.292 ± 0.040 to 119.723 ± 0.036 Ma and suggest a duration of 576 ± 45 k.y. Bayesian modeling of these dates collectively supports a duration of 540 ± 37 k.y., which represents a minimum duration of the reversed polarity interval. Our estimates for the minimum duration of the reversed polarity interval in China are comparable to those of Malinverno et al. (2010, 2012) and Leandro et al. (2022). Importantly, each of these age models, including our Bayesian-radioisotopic model (Fig. 2), supports a duration much longer than the “ISEA” event.

Despite radioisotopic dating at globally distributed sites, constraints on chron M0r have been imprecise, leaving chronostratigraphic and magnetostratigraphic correlations uncertain (Fig. 3; Table S2). For instance, Mahoney

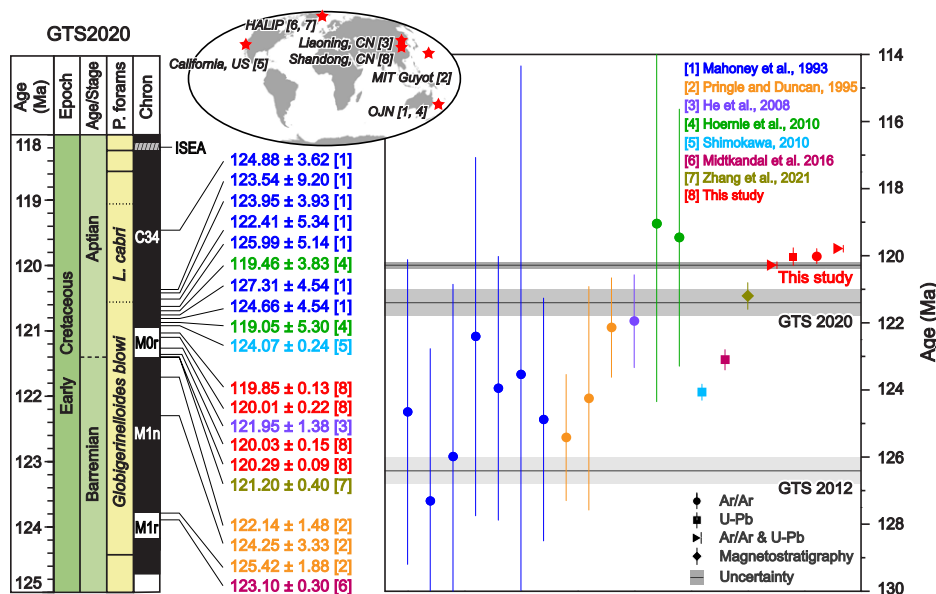


Figure 3. Comparison of $^{40}\text{Ar}/^{39}\text{Ar}$ and U-Pb ages with paleomagnetic information constraining chron M0r. Radioisotopic dates (Ma) are annotated in Geologic Time Scale (GTS) 2020 (Gale et al., 2020; Ogg, 2020). Data are from Table S2 (2σ external uncertainties; see text footnote 1). HALIP—High Arctic large igneous province; CN—China; OJN—Ontong Java Nui; P. forams—planktonic foraminifera; L.—*Leupoldina*.

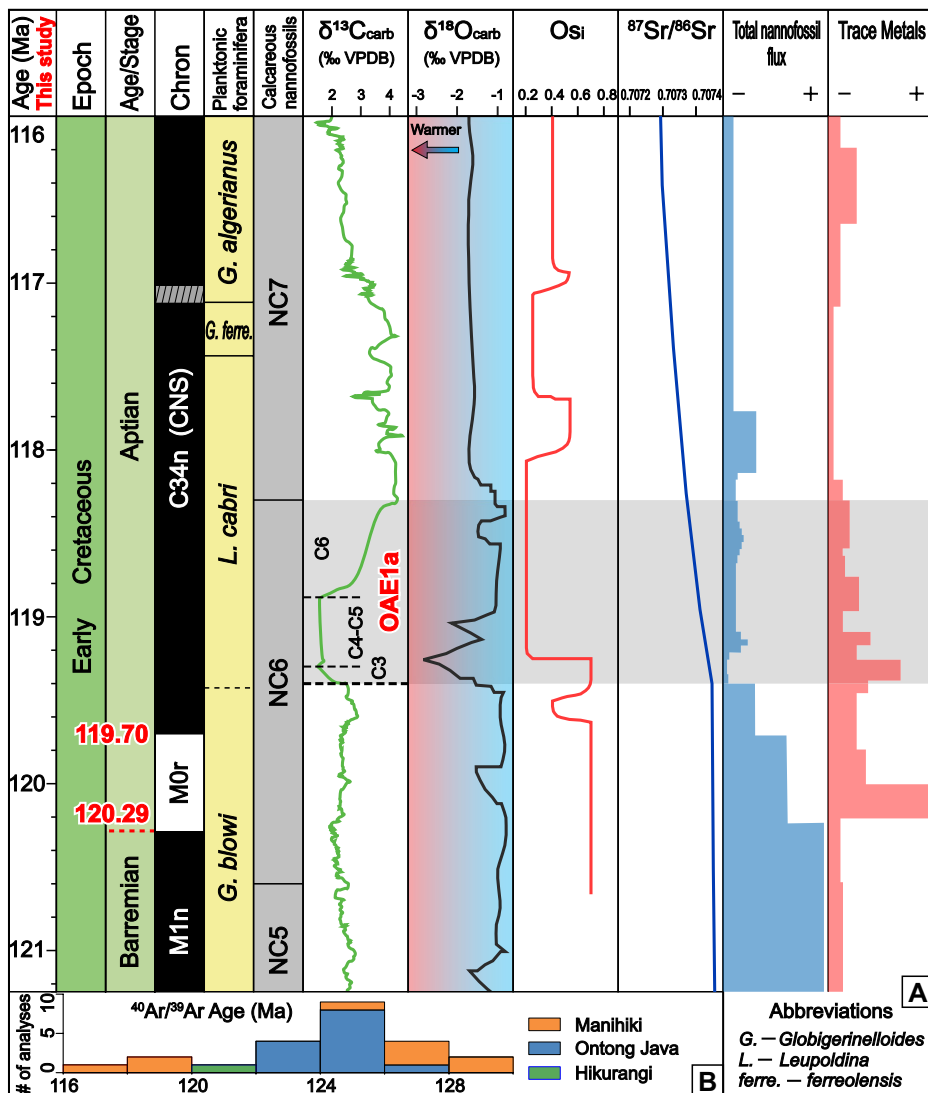


Figure 4. (A) Proposed age model for onset of chron M0r translates to change in onset of Cretaceous normal superchron, oceanic anoxic event 1a (OAE 1a), and salient geochemical and paleobiologic proxies. Foraminifera, nannofossil, $\delta^{13}\text{C}_{\text{carb}}$, and $\delta^{18}\text{O}_{\text{carb}}$ data are based on Geologic Time Scale 2020 (Gale et al., 2020; Ogg, 2020). Os isotopes are after Tejada et al. (2009) and Matsumoto et al. (2021). Sr isotopes are after Bralower et al. (1997). Total nannofossil flux and trace metals are after Erba et al. (2015). VPDB—Vienna Peedee belemnite. (B) Range of Ontong Java Nui (OJN) ages; $^{40}\text{Ar}/^{39}\text{Ar}$ data are from Table S2 (see text footnote 1). Os, $^{187}\text{Os}/^{188}\text{Os}$.

et al. (1993) reported seven whole-rock $^{40}\text{Ar}/^{39}\text{Ar}$ ages with 2σ internal uncertainties of 3%–7% from Ontong Java Plateau (OJP) basalts and suggested that they correspond to the CNS to give a minimum age for chron M0r of 124.8 Ma. Reversely magnetized lavas in China, $^{40}\text{Ar}/^{39}\text{Ar}$ dated by He et al. (2008), place the base of the Aptian at 121.95 ± 1.38 Ma. Zhang et al. (2021) proposed an interpolated age of 121.2 ± 0.4 Ma for the base of M0r using magnetostratigraphy from boreholes in Svalbard, Norway, combined with a U-Pb CA-ID-TIMS date of 123.10 ± 0.30 Ma for the uppermost part of magnetochron M1r (Midt-kandal et al., 2016). The interpolated age of Zhang et al. (2021) was adopted in the current GTS 2020 (Gale et al., 2020; Ogg, 2020), which places the base of the Aptian at 121.2 ± 0.4 Ma.

The GTS 2020 age contrasts with the $^{40}\text{Ar}/^{39}\text{Ar}$ ages of reversely magnetized lavas in the MIT Guyot in the northwestern Pacific Ocean (Pringle and Duncan, 1995) and the astrochronology of the Piobbico core, central Italy (Huang et al., 2010), both of which were used in GTS 2012 to place the base of the Aptian at 126.3 ± 0.4 Ma (Gradstein et al., 2012). Therefore, radioisotopic ages do not directly date the base of M0r at any of these sites. Astronomical tuning of the Poggio le Guaine core, Italy, implies an age of ca. 120.2 Ma for the Barremian-Aptian boundary; however, this age model (Leandro et al., 2022), like those of Huang et al. (2010), was not anchored to radioisotopic age determinations, so uncertainties are difficult to estimate.

Our age of 120.287 ± 0.088 Ma for the ZY18-04 tuff provides the most unambiguous

radioisotopic constraint for the onset of chron M0r. Combined with the duration of 590 ± 82 k.y. suggested by Malinverno et al. (2012), the termination age of M0r is revised to 119.697 ± 0.120 Ma (Fig. 4). In turn, a 119.697 ± 0.120 Ma age for the base of the CNS implies a duration for chron C34n of ~ 36 m.y., or ~ 1 m.y. shorter than that given in GTS 2020. This revised duration suggests that the average sea-floor spreading rate during the CNS interval was $\sim 3.5\%$ higher than that implied by GTS 2020.

OAE 1a reflects a major perturbation of the global carbon cycle, characterized by a sharp negative carbon isotope excursion, followed by a prolonged positive excursion (Fig. 4A; e.g., Castro et al., 2021). The negative carbon excursion likely records massive input of light carbon into the atmosphere-marine system. However, debates as to the sources of carbon focus on submarine volcanism, methane release, or the intrusion of magma into organic-rich sediments in the High Arctic large igneous province (HALIP) (e.g., Méhay et al., 2009; Polteau et al., 2016; Adloff et al., 2020; Jiang et al., 2022). A volcanic driver is supported by geochemical and biotic changes (Fig. 4A). For instance, Os and Sr isotopes record an abrupt shift to unradiogenic values, implying mantle-derived volcanic-hydrothermal input (Matsumoto et al., 2021; Martínez-Rodríguez et al., 2021). A decline in nannofossil abundance and peak in trace metal concentrations in marine sediment further suggest a volcanic driver (Erba et al., 2015). Additionally, the oldest sediment overlying the capping OJP basalts in cores from Ocean Drilling Program Leg 192 comprises the upper part of the *Leupoldina cabri* foraminiferal zone and exhibits a prominent positive $\delta^{13}\text{C}$ shift (Sikora and Bergen, 2004). This indicates that eruption of the main OJP lavas continued during much of OAE 1a, consistent with the idea that formation of the plateau was a potential cause of anoxia (e.g., Larson and Erba, 1999). The strength of the correlations between sedimentary archives of OAE 1a and submarine volcanism remains weak, however, owing to the paucity and questionable accuracy of the ca. 129–118 Ma $^{40}\text{Ar}/^{39}\text{Ar}$ ages from the Ontong Java Nui Plateau, many of which were obtained decades ago and have uncertainties of ± 2 –6 Ma (Fig. 4B; Table S2).

The astronomical age model of Malinverno et al. (2010) from the Cismont APTICORE suggests that OAE 1a lasted 1.11 ± 0.11 m.y. and began 298 ± 15 k.y. following termination of chron M0r. Coupling our new radioisotopic age for the termination of M0r at 119.70 ± 0.12 Ma with the age model of Malinverno et al. (2012) leads to an estimate that OAE 1a occurred between 119.40 ± 0.12 and 118.29 ± 0.16 Ma. Astronomical tuning of the Poggio le Guaine core suggests a slightly shorter duration of ~ 920 k.y. (Leandro et al., 2022), which does not significantly change this inter-

pretation. These findings provide a firm chronostratigraphic framework for OAE 1a against which the veracity of correlation with Ontong Java Nui volcanism can be rigorously tested.

CONCLUSIONS

A high-resolution chronostratigraphic framework for the Qingshan Group in the Jiaolai Basin, eastern China, tightly constrains the timing and minimum duration of reversed polarity chron M0r. Bayesian age modeling of U-Pb zircon and $^{40}\text{Ar}/^{39}\text{Ar}$ sanidine dates suggests an M0r duration of 540 ± 37 k.y. This indicates that the period of reversed polarity corresponds to chron M0r rather than “M-1r,” which supports the astrochronologic age model of Malinverno et al. (2012) for M-sequence seafloor magnetic anomalies. An integrated U-Pb and $^{40}\text{Ar}/^{39}\text{Ar}$ age constrains the onset of chron M0r to $120.29 [\pm 0.09]$ Ma, which is ~ 1 m.y. younger than that in GTS 2020 (Gale et al., 2020). Our onset age for chron M0r implies that the CNS began at $119.70 [\pm 0.12]$ Ma. Thus, the seafloor spreading rate estimate for this period in GTS 2020 is $\sim 3.5\%$ too low. Moreover, we propose that OAE 1a occurred between $119.40 [\pm 0.12]$ and $118.29 [\pm 0.16]$ Ma, which provides a basis for testing hypothesized triggers, including Ontong Java Nui volcanism, methane release, or HALIP emplacement.

ACKNOWLEDGMENTS

We thank Editor William Clyde and reviewers James Ogg, José Castro, and Alberto Malinverno for their constructive suggestions, and Bryan Wathen and Ben Bruck for laboratory assistance. This work was supported by National Natural Science Foundation of China grants 42288201 and 41425013, Strategic Priority Research Program B of the Chinese Academy of Sciences (XDB 18030505), and U.S. National Science Foundation grant EAR-1951812.

REFERENCES CITED

- Adloff, M., Greene, S.E., Parkinson, I.J., Naafs, B.D.A., Preston, W., Ridgwell, A., Lunt, D.J., Jiménez, J.M.C., and Monteiro, F.M., 2020, Unravelling the sources of carbon emissions at the onset of oceanic anoxic event (OAE) 1a: Earth and Planetary Science Letters, v. 530, <https://doi.org/10.1016/j.epsl.2019.115947>.
- Bralower, T.J., Fullagar, P.D., Paull, C.K., Dwyer, G.S., and Leckie, R.M., 1997, Mid-Cretaceous strontium-isotope stratigraphy of deep-sea sections: Geological Society of America Bulletin, v. 109, p. 1421–1442, [https://doi.org/10.1130/0016-7606\(1997\)109<1421:MCSISO>2.3.CO;2](https://doi.org/10.1130/0016-7606(1997)109<1421:MCSISO>2.3.CO;2).
- Castro, J.M., Ruiz-Ortiz, P.A., de Gea, G.A., Aguado, R., Jarvis, I., Weissert, H., Molina, J.M., Nieto, L.M., Pancost, R.D., Quijano, M.L., and Reolid, M., 2021, High-resolution C-isotope, TOC and biostratigraphic records of OAE 1a (Aptian) from an expanded hemipelagic cored succession, western Tethys: A new stratigraphic reference for global correlation and paleoenvironmental reconstruction: Palaeogeography and Palaeoclimatology, v. 36, <https://doi.org/10.1029/2020PA004004>.
- Chambers, L.M., Pringle, M.S., and Fitton, J.G., 2004, Phreatomagmatic eruptions on the Ontong Java Plateau: An Aptian $^{40}\text{Ar}/^{39}\text{Ar}$ age for volcanic clastic rocks at ODP Site 1184, in Fitton, J.G., et al., eds., Origin and Evolution of the Ontong Java Plateau: Geological Society, London, Special Publication 229, p. 325–331, <https://doi.org/10.1144/GSL.SP.2004.229.01.18>.
- Cronin, M., Tauxe, L., Constable, C., Selkin, P., and Pick, T., 2001, Noise in the quiet zone: Earth and Planetary Science Letters, v. 190, p. 13–30, [https://doi.org/10.1016/S0012-821X\(01\)00354-5](https://doi.org/10.1016/S0012-821X(01)00354-5).
- Erba, E., Duncan, R.A., Bottini, C., Tiraboschi, D., Weissert, H., Jenkyns, H.C., and Malinverno, A., 2015, Environmental consequences of Ontong Java Plateau and Kerguelen Plateau volcanism: Geological Society of America Special Paper 511, p. 271–303, [https://doi.org/10.1130/2015.2511\(15\)](https://doi.org/10.1130/2015.2511(15)).
- Gale, A.S., Mutterlose, J., and Batenburg, S., 2020, The Cretaceous Period, in Gradstein, F.M., Ogg, J.G., Schmitz, M.D., and Ogg, G.M., eds., The Geologic Time Scale 2020, Volume 2: Amsterdam, Netherlands, Elsevier, p. 1023–1086, <https://doi.org/10.1016/B978-0-12-824360-2.00027-9>.
- Gradstein, F.M., Ogg, J.G., Schmitz, M.D., and Ogg, G.M., eds., 2012, The Geologic Time Scale 2012: Amsterdam, Netherlands, Elsevier, 1176 p.
- He, H.Y., Pan, Y.X., Tauxe, L., Qin, H.F., and Zhu, R.X., 2008, Toward age determination of the M0r (Barremian-Aptian boundary) of the Early Cretaceous: Physics of the Earth and Planetary Interiors, v. 169, p. 41–48, <https://doi.org/10.1016/j.pepi.2008.07.014>.
- Helsley, C.E., and Steiner, M.B., 1968, Evidence for long intervals of normal polarity during the Cretaceous Period: Earth and Planetary Science Letters, v. 5, p. 325–332, [https://doi.org/10.1016/S0012-821X\(68\)80060-3](https://doi.org/10.1016/S0012-821X(68)80060-3).
- Hoernle, K., Hauff, F., Van den Bogaard, P., Werner, R., Mortimer, N., Geldmacher, J., Garbe-Schönberg, D., and Davy, B., 2010, Age and geochemistry of volcanic rocks from the Hikurangi and Manihiki oceanic Plateaus: Geochimica et Cosmochimica Acta, v. 74, p. 7196–7219, <https://doi.org/10.1016/j.gca.2010.09.030>.
- Huang, C.J., Hinnov, L.A., Fischer, A.G., Grippo, A., and Herbert, T., 2010, Astronomical tuning of the Aptian Stage from Italian reference sections: Geology, v. 38, p. 899–902, <https://doi.org/10.1130/G31177.1>.
- Jiang, Q., Jourdan, F., Olierook, H.K., Merle, R.E., Bourdet, J., Fougereuse, D., Godel, B., and Walker, A.T., 2022, Volume and rate of volcanic CO₂ emissions governed the severity of past environmental crises: Proceedings of the National Academy of Sciences of the United States of America, v. 119, <https://doi.org/10.1073/pnas.2202039119>.
- Keating, B.H., and Helsley, C.E., 1978, Paleomagnetic results from DSDP Hole 391C and the magnetostratigraphy of Cretaceous sediments from the Atlantic Ocean floor, in Benson, W.E., Sheridan, R.E., et al., Initial Reports of the Deep Sea Drilling Project, Volume 44: Washington, D.C., U.S. Government Printing Office, p. 523–528, <https://doi.org/10.2973/dsdp.proc.44.113.1978>.
- Larson, R.L., and Erba, E., 1999, Onset of the mid-Cretaceous greenhouse in the Barremian-Aptian: Igneous events and the biological, sedimentary, and geochemical responses: Palaeogeography, v. 14, p. 663–678, <https://doi.org/10.1029/1999PA900040>.
- Leandro, C.G., Savian, J.F., Kochhann, M.V.L., Franco, D.R., Coccioni, R., Frontalini, F., Gardin, S., Jovane, L., Figueiredo, M., Tedeschi, L.R., and Janikian, L., 2022, Astronomical tuning of the Aptian Stage and its implications for age recalibrations and paleoclimatic events: Nature Communications, v. 13, p. 1–12, <https://doi.org/10.1038/s41467-022-30075-3>.
- Mahoney, J.J., Storey, M., Duncan, R.A., Spencer, K.J., and Pringle, M., 1993, Geochemistry and age of the Ontong Java Plateau, in Pringle, M.S., et al., eds., The Mesozoic Pacific: Geology, Tectonics, and Volcanism: American Geophysical Union Geophysical Monograph 77, p. 233–261, <https://doi.org/10.1029/GM077p0233>.
- Malinverno, A., Erba, E., and Herbert, T.D., 2010, Orbital tuning as an inverse problem: Chronology of the early Aptian oceanic anoxic event 1a (Selli level) in the Cismon APTICORE: Palaeogeography, v. 25, PA2203, <https://doi.org/10.1029/2009PA001769>.
- Malinverno, A., Hildebrandt, J., Tominaga, M., and Channell, J.E.T., 2012, M-sequence geomagnetic polarity time scale (MHTC12) that steadies global spreading rates and incorporates astrochronology constraints: Journal of Geophysical Research, v. 117, B06104, <https://doi.org/10.1029/2012JB009260>.
- Martínez-Rodríguez, R., Selby, D., Castro, J.M., de Gea, G.A., Nieto, L.M., and Ruiz-Ortiz, P.A., 2021, Tracking magmatism and oceanic change through the early Aptian anoxic event (OAE 1a) to the late Aptian: Insights from osmium isotopes from the westernmost Tethys (SE Spain) Cau core: Global and Planetary Change, v. 207, <https://doi.org/10.1016/j.gloplacha.2021.103652>.
- Matsumoto, H., Coccioni, R., Frontalini, F., Shirai, K., Jovane, L., Trindade, R., Savian, J.F., Tejada, M.L.G., Gardin, S., and Kuroda, J., 2021, Long-term Aptian marine osmium isotopic record of Ontong Java Nui activity: Geology, v. 49, p. 1148–1152, <https://doi.org/10.1130/G48863.1>.
- Méhay, S., Keller, C.E., Bernasconi, S.M., Weissert, H., Erba, E., Bottini, C., and Hochuli, P.A., 2009, A volcanic CO₂ pulse triggered the Cretaceous oceanic anoxic event 1a and a biocalcification crisis: Geology, v. 37, p. 819–822, <https://doi.org/10.1130/G30100A.1>.
- Midtkandal, I., Svensen, H.H., Planke, S., Corfu, F., Polteau, S., Torsvik, T.H., Faleide, J.I., Grundvåg, S.A., Selnes, H., Kürschner, W., and Olausson, S., 2016, The Aptian (Early Cretaceous) oceanic anoxic event (OAE1a) in Svalbard, Barents Sea, and the absolute age of the Barremian-Aptian boundary: Palaeogeography, Palaeoclimatology, Palaeoecology, v. 463, p. 126–135, <https://doi.org/10.1016/j.palaeo.2016.09.023>.
- Ogg, J.G., 2012, Geomagnetic polarity time scale, in Gradstein, F.M., Ogg, J.G., Schmitz, M.D., and Ogg, G.M., eds., The Geologic Time Scale 2012, Volume 1: Amsterdam, Netherlands, Elsevier, p. 85–113, <https://doi.org/10.1016/B978-0-444-59425-9.00005-6>.
- Ogg, J.G., 2020, Geomagnetic polarity time scale, in Gradstein, F.M., Ogg, J.G., Schmitz, M.D., and Ogg, G.M., eds., The Geologic Time Scale 2020, Volume 1: Amsterdam, Netherlands, Elsevier, p. 159–192, <https://doi.org/10.1016/B978-0-12-824360-2.00005-X>.
- Olierook, H.K.H., Jourdan, F., and Merle, R.E., 2019, Age of the Barremian-Aptian boundary and onset of the Cretaceous normal superchron: Earth-Science Reviews, v. 197, <https://doi.org/10.1016/j.earscirev.2019.102906>.
- Polteau, S., Hendriks, B.W., Planke, S., Ganerød, M., Corfu, F., Faleide, J.I., Midtkandal, I., Svensen, H.S., and Myklebust, R., 2016, The Early Cretaceous Barents Sea sill complex: Distribution, $^{40}\text{Ar}/^{39}\text{Ar}$ geochronology, and implications for carbon gas formation: Palaeogeography, Palaeoclimatology, Palaeoecology, v. 441, p. 83–95, <https://doi.org/10.1016/j.palaeo.2015.07.007>.

- Pringle, M., and Duncan, R., 1995, Radiometric ages of basement lavas recovered at Loen, Wodejebato, MIT, and Takuyo-Daisan Guyots, northwestern Pacific Ocean, *in* Haggerty, J.A., Premoli Silva, I., Rack, F., and McNutt, M.K., eds., *Proceedings of the Ocean Drilling Program, Scientific Results Volume 144: College Station, Ocean Drilling Program*, p. 547–557, <https://doi.org/10.2973/odp.proc.sr.144.033.1995>.
- Qin, H.F., Hao, W.X., Deng, C.L., Zhao, P., Shen, Z.S., Han, F., He, H.Y., Pan, Y.X., and Zhu, R.X., 2022, Sinistral displacement along the Tan-Lu fault during the Cretaceous induced by Paleo-Pacific subduction: Constraints from new paleomagnetic and U-Pb geochronological data: *Journal of Asian Earth Sciences*, v. 237, <https://doi.org/10.1016/j.jseas.2022.105362>.
- Santosh, M., 2010, Supercontinent tectonics and biogeochemical cycle: A matter of ‘life and death’: *Geoscience Frontiers*, v. 1, p. 21–30, <https://doi.org/10.1016/j.gsf.2010.07.001>.
- Shimokawa, A., 2010, Zircon U-Pb Geochronology of the Great Valley Group: Recalibrating the Lower Cretaceous Time Scale [M.S. thesis]: University of North Carolina at Chapel Hill, 46 p.
- Sikora, P.J., and Bergen, J.A., 2004, Lower Cretaceous planktonic foraminiferal and nannofossil biostratigraphy of Ontong Java Plateau sites from DSDP Leg 30 and ODP Leg 192, *in* Fitton, J.G., Mahoney, J.J., Wallace, P.J., and Saunders, A.D., eds., *Origin and Evolution of the Ontong Java Plateau: Geological Society, London, Special Publication 229*, p. 83–111, <https://doi.org/10.1144/GSL.SP.2004.229.01.07>.
- Tarduno, J.A., 1990, Brief reversed polarity interval during the Cretaceous normal polarity superchron: *Geology*, v. 18, p. 683–686, [https://doi.org/10.1130/0091-7613\(1990\)018<0683:BRP IDT>2.3.CO;2](https://doi.org/10.1130/0091-7613(1990)018<0683:BRP IDT>2.3.CO;2).
- Tejada, M.L.G., Suzuki, K., Kuroda, J., Coccioni, R., Mahoney, J.J., Ohkouchi, N., Sakamoto, T., and Tatsumi, Y., 2009, Ontong Java Plateau eruption as a trigger for the early Aptian oceanic anoxic event: *Geology*, v. 37, p. 855–858, <https://doi.org/10.1130/G25763A.1>.
- Trayler, R.B., Schmitz, M.D., Cuitiño, J.I., Kohn, M.J., Bargo, M.S., Kay, R.F., Strömberg, C.A.E., and Vizcaíno, S.F., 2020, An improved approach to age-modeling in deep time: Implications for the Santa Cruz Formation, Argentina: *Geological Society of America Bulletin*, v. 132, p. 233–244, <https://doi.org/10.1130/B35203.1>.
- VandenBerg, J., Klootwijk, C.T., and Wonders, A.A.H., 1978, Late Mesozoic and Cenozoic movements of the Italian peninsula: further paleomagnetic data from the Umbrian sequence: *Geological Society of America Bulletin*, v. 89, p. 133–150, [https://doi.org/10.1130/0016-7606\(1978\)89<133:LMACMO>2.0.CO;2](https://doi.org/10.1130/0016-7606(1978)89<133:LMACMO>2.0.CO;2).
- Zhang, Y., Ogg, J.G., Minguez, D., Hounslow, M.W., Olausson, S., Gradstein, F.M., and Esmeray-Senlet, S., 2021, Magnetostratigraphy of U-Pb-dated boreholes in Svalbard, Norway, implies that magnetochron M0r (a proposed Barremian-Aptian boundary marker) begins at 121.2 ± 0.4 Ma: *Geology*, v. 49, p. 733–737, <https://doi.org/10.1130/G48591.1>.
- Zhang, Y.Q., Dong, S.W., and Shi, W., 2003, Cretaceous deformation history of the middle Tan-Lu fault zone in Shandong Province, eastern China: *Tectonophysics*, v. 363, p. 243–258, [https://doi.org/10.1016/S0040-1951\(03\)00039-8](https://doi.org/10.1016/S0040-1951(03)00039-8).

Printed in USA